J. Quant. Spectrosc. Radiat. Transfer Vol. 40, No. 1, pp. 51–69, 1988
Printed in Great Britain.

0022-4073/88 $3.00 + 0.00

ALGORITHMS FOR RADIATIVE INTENSITY CALCULATIONS IN MODERATELY THICK ATMOSPHERES USING A TRUNCATION APPROXIMATION

T. NAKAJIMA† and M. TANAKA
Upper Atmosphere Research Laboratory, Tohoku University, Sendai 980, Japan

(*Received* 10 *August* 1987; *received for publication* 6 *January* 1988)

Abstract—The efficiency of numerical calculations is discussed for selected algorithms employing the discrete ordinate method and the truncation approximation for the solar radiative intensity in moderately thick, plane-parallel scattering atmospheres. It is found that truncation of the phase function causes a significant error in the computed intensity and the magnitude of this error depends significantly on how the intensity is retrieved from the truncated radiative transfer equation. A newly developed retrieval algorithm, the IMS-method, yields the intensity field with an error $\lesssim 1\%$ when the number of discrete paths is as small as 10 in the hemisphere for aerosol-laden atmospheres with optical thickness $\lesssim 1$.

1. INTRODUCTION

New techniques for solving the solar radiative transfer equation in a plane-parallel atmosphere have improved the stability and accuracy of numerical evaluations of the radiative energy flux considerably. For example, refinements of the discrete ordinates and spherical harmonics methods[1–6] provide a stable algorithm for the solution of any optical stratification in atmospheric scattering. The delta-M method of Wiscombe[7] is a suitable truncation algorithm for a strongly anisotropic phase function. These algorithms and important recent advances in computer capability allow easy application for accurate radiative flux computations.

For the solution of the radiative intensity field, however, accurate calculations are time-consuming in spite of these algorithms. The strongly peaked phase functions of clouds, aerosols and hydrosols require a large number of discrete paths in the discrete ordinates or matrix operator methods, especially for calculations of the solar aureole. Stamnes and Dale[8] showed that the discrete ordinates method attains an accuracy of better than 1% for Deirmendjian's Haze-L polydispersion for the number of discrete paths as large as 24 in the hemisphere. It is noteworthy, however, that the Haze-L size distribution has a phase function with a relatively small forward peak. For other phase functions which are more strongly peaked in the forward direction, more streams are necessary for accurate calculations of the intensity. There have been few investigations of the efficiency of intensity calculation algorithms after the development of the delta-M method, while recently improved opto-electrical devices are supplying large amount of high quality data of the intensity to be analyzed in the field of remote sensing from the ground, aircraft and satellites. In these circumstances, it will be very useful to develop an accurate, yet economical, algorithm for the radiative intensity calculations.

Recently, Nakajima et al[9] and Arao and Tanaka[10] developed schemes for calculating intensity in the solar aureole region. The former is an improved version of the truncation method of Potter[11] and the latter is an improved version of Deirmendjian's perturbation theory.[12,13] In this paper, we analyze the advantages and disadvantages of several algorithms for intensity calculations, and develop an improved method for calculating both the transmitted and reflected radiative intensities. These methods are applicable to various emergent angles, as well as in the solar aureole region, and make use of the discrete ordinates method and the truncation approximation.

†Address for correspondence: Climate and Radiation Branch, Code 613, Laboratory for Atmospheres, Goddard Space Flight Center, Greenbelt, MD 20771, U.S.A.

Although any desired accuracy can be attained by existing algorithms with a sufficiently large number of discrete paths, an exceedingly high accuracy seems to be unimportant in remote sensing applications because uncertainties involved in measuring the radiative intensity and in atmospheric variability are as large as several percent for almost all applications. Inversion algorithms for retrieving the aerosol volume spectrum from the circumsolar intensity field show that an agreement between data and retrieved values is usually between 1 and 5%, but this disagreement is unavoidable due to horizontal inhomogeneity in the atmosphere.[14,15]

As a scope of the present paper, therefore, we restrict our discussion to the development of an algorithm for computing the radiative intensity to an accuracy of $\sim 1\%$. We also restrict our applications to the scattering problem in a cloudless aerosol-laden atmosphere with an optical thickness $\lesssim 1$, because calculations of the intensity field in such a moderately thick atmosphere is difficult, and an efficient method for the problem will be different from that in an optically thick cloudy atmosphere where an asymptotic property of the radiative field dominates.[16,17]

2. THEORETICAL CONSIDERATION

The basic equation for our discussion is the transfer equation for diffuse solar radiation in a plane-parallel scattering atmosphere,

$$\mu \, du(\tau, \Omega)/d\tau = -u(\tau, \Omega) + \omega \int d\Omega' \, P(\Omega \cdot \Omega') u(\tau, \Omega') + \omega P(\Omega \cdot \Omega_0) \exp(-\tau/\mu_0) F_0, \tag{1}$$

where the angular integral is defined by

$$\int d\Omega' = \int_{-1}^{1} d\mu' \int_{0}^{2\pi} d\phi',$$

$u(\tau, \Omega)$is the specific intensity at the optical depth τ along the unit vector Ω in the direction (μ, ϕ), μ and ϕ are the cosine of the nadir angle and the azimuthal angle, respectively, and ω and P represent the single-scattering albedo and phase function of the air mass, respectively. The last term on the right-hand side represents the diffuse intensity arising from single scattering of the incident solar beam F_0 from the direction Ω_0 into the direction Ω. Hereafter, we represent Eq. (1) by the functional notation $\mathscr{T}(u, \omega P, \tau)$. Since the phase function for particulate matter has a strongly peaked forward spike formed by light diffraction, very fine angular resolution is required for accurate evaluation of the integral in Eq. (1). To reduce this computational burden, a truncation approximation has traditionally been used. In the truncation approximation, we approximate the phase function as a sum of a delta function and a truncated function,

$$P(x) \approx \frac{f}{2\pi} \delta(1 - x) + (1 - f) P^*(x), \tag{2}$$

where f is the truncation fraction and x is the cosine of the scattering angle Θ. Introducing the scaled variables

$$d\tau^* = (1 - f\omega) \, d\tau \quad \text{and} \quad \omega^* = (1 - f)\omega/(1 - f\omega), \tag{3}$$

we have a truncated transfer equation $\mathscr{T}(u^*, \omega^* P^*, \tau^*)$ in the same form as in Eq. (1) but with the scaled variables and the truncated phase function P^*. In the following, we present several algorithms which may be used to retrieve the intensity field of the original transfer equation from the truncated equation.

2.1. The DM-method

A well-defined and automatic truncation algorithm, the delta-M method, was introduced by Wiscombe[7] as a functional equality, i.e., conservation of the moment g_n of the expansion of the phase function by Legendre polynomial $P_n(x)$,

$$P_L(x, g, M) = \frac{1}{4\pi} \sum_{n=0}^{M} (2n + 1) g_n P_n(x). \tag{4}$$

If we want to truncate the phase function at a truncation order M^*, the truncated phase function P^* is uniquely given by the moment and fraction

$$g_n^* = (g_n - f)/(1 - f) \quad \text{and} \quad f = g_{M^*+1} \tag{5}$$

by using the following functional equality deduced from Eq. (2):

$$P_L(x, g, M^* + 1) = fP_L(x, 1, M^* + 1) + (1 - f)P_L(x, g^*, M^*). \tag{6}$$

In the discrete ordinates and matrix operator methods using the Gaussian quadrature of order $2N$, the angular integral term in Eq. (1) is precisely evaluated by the discrete quadrature for a phase function with $M \leqslant 2N - 1$ within an approximation of the intensity expressed by a Legendre series with $M \leqslant 2N$.[18] Using the delta-M method, therefore, the transfer equation can be solved for a reasonable number N of discrete paths of the emergent zenith angle if we use the transfer equation with the scaled variables and the truncated phase function $P^*(x) = P_L(x, g^*, M^*)$.

The profile labelled DM in Fig. 1 shows an example of truncation by the delta-M method with $N = 10$ for JUNGE-3 polydispersion defined in the following section. As is shown in Fig. 1, the truncated phase function fluctuates around the original function. Large positive deviations appear around transient scattering angles for which the forward peak becomes less dominant, because of the approximation of the forward peak by the delta function. This result follows because the delta function has larger moments than those of the forward peak, and thus the conservation rule of the moment in Eq. (6) yields a truncated profile larger than the original value in the transient region.

Although the conservation rule in the delta-M method assures the accuracy of the radiative flux, which is an angular integral of the intensity, the intensity field itself fluctuates as shown in the right-hand portion (labelled DM) of Fig. 2. This figure shows the relative error in the intensity calculated by the discrete ordinates method for normal incidence and the phase function truncated by the delta-M method with $N = 10$ and with an aerosol optical thickness $\tau_a = 0.8$. Hereafter, we will refer to this algorithm for computing the intensity as the DM-method. Detailed information

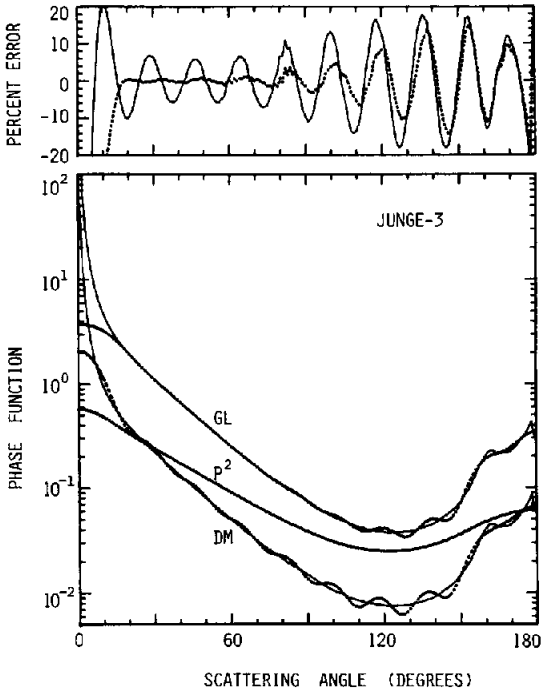

Fig. 1. Phase functions truncated by the delta-M method (labelled DM), Gaussian–Legendre expansion method (labelled GL and shifted upward by a factor of 5) for JUNGE-3 polydispersion, and the effective phase function for secondary scattering (labelled P^2) for the truncated phase function DM. The percent deviation is shown between the truncated and original functions in the upper figure (the solid line refers to DM and the broken line to GL).

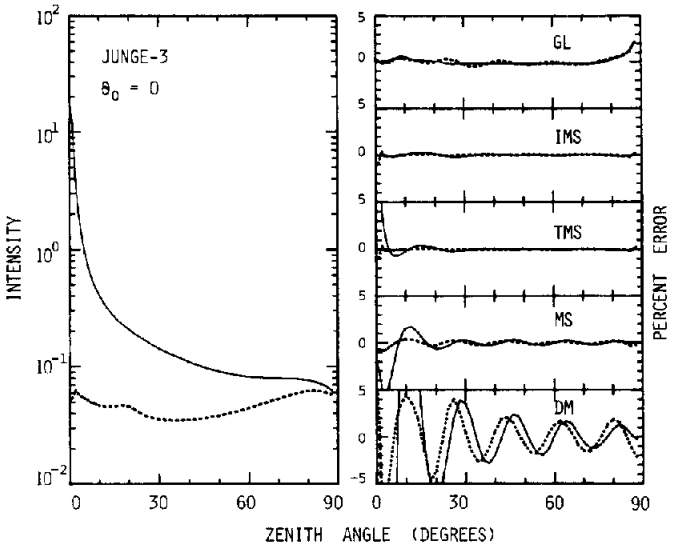

Fig. 2. The exact intensity field (left segment) and percentage errors in the various algorithms with $N = 10$ (right segments) as a function of emergent zenith angle for the case $\theta_0 = 0°$, $\tau_a = 0.8$ and JUNGE-3 polydispersion. The solid lines refer to transmission and the broken lines to reflection.

on the simulation is presented in the following section. Since the phase function has a sharp forward peak, the magnitude of the intensity ranges over two orders of magnitude (cf. Fig. 2). Even for such a strongly anisotropic intensity field, the DM-method yields the intensity to an accuracy of several percent outside the solar aureole region. We observe, however, that the fluctuation of the percentage error in Fig. 2 is a result of the fluctuation in the truncated phase function labelled DM in Fig. 1. Therefore, to suppress this fluctuation, similarity between the truncated and original phase functions will be important in determining the accuracy of the intensity calculation, as is discussed in the following method.

2.2. The GL-method

Historically, the truncation approximation originated from a decomposition of the phase function into a forward peak $\hat{P}$ and the residue P^* as follows:

$$P(x) = f\hat{P}(x) + (1 - f)P^*(x). \tag{7}$$

After the decomposition, the spike $\hat{P}(x)$ is approximated by the delta function. Potter[11] truncated the sharp forward diffraction peak of a cloud phase function by a log-linear extrapolation function, and Tanaka and Nakajima[19] truncated the broad forward peak of a hydrosol phase function by a Lorentzian profile. With these classical methods, determinations of the fraction and the extrapolation function are dependent on the shape of each phase function. Nakajima et al[9] used the delta-M method as a guide in approximating the phase function by a sum of the Gaussian function and a series of Legendre polynomial, as shown by the profile labelled GL in Fig. 1. Thus,

$$P(x) \approx fP_G(x) + (1 - f)P_L(x, g^*, 2N - 1), \tag{8}$$

where

$$P_G(x) = \sum_n C_n \exp(-\Theta^2/E_n). \tag{9}$$

In this method, the forward peak is preliminarily truncated by the delta-M method with moments g'^* and a truncation order M^* about N before the Gaussian fitting

$$fP_G(x) \approx P(x) - (1 - f)P_L(x, g'^*, N). \tag{10}$$

With this procedure, deviation of the truncated profile from the original profile is considerably suppressed at the transient scattering angles, in spite of the fact that the truncation order M^* reduces to N, which is different from $2N-1$ in the DM-method. This method of truncation is a classical one guided by the delta-M method. With the approximation of Eq. (8), the transfer equations for the truncated and forward parts of the phase function can be independently solved by the discrete ordinate method and the small angle approximation of Weinman et al,[20] respectively. Modifying the original paper,[9] we subtract the singly-scattered intensity obtained in this method and add the exact single scattering solution u_1 calculated from the following equation $\mathscr{T}_1(u_1, \omega P, \tau)$, thereby removing undesired errors involved in the Gaussian fitting in Eq. (10):

$$\mu \, \mathrm{d}u_1(\tau, \Omega)/\mathrm{d}\tau = -u_1(\tau, \Omega) + \omega P(\Omega \cdot \Omega_0)\exp(-\tau/\mu_0)F_0 \tag{11}$$

or

$$u_1(\tau, \Omega) = \frac{\exp(-\tau/\mu)}{|\mu|} F_0 \sum_{l=1}^{L} \omega_l P^{(l)}(\Omega \cdot \Omega_0) \int_{\tau_{l-1}}^{\tau_l} \mathrm{d}t \, \exp[(1/\mu - 1/\mu_0)t]. \tag{12}$$

In Eq. (12) we assume L homogeneous atmospheric layers between τ and τ_L for reflection ($\mu < 0$) and between 0 and τ for transmission ($\mu > 0$), and ω_l and $P^{(l)}$ represent the single-scattering albedo and phase function of the lth layer, respectively.

The error in the intensity calculated by the indicated algorithm (hereafter referred to as the GL-method) is shown in the segment of Fig. 2 labelled GL. Although the GL-method induces a systematic error near the horizon because of a breakdown of moment conservation, the overall accuracy is better than for the DM-method. This result follows because the truncated phase function does not deviate strongly from the original phase function at large scattering angles and multiple scattering has been taken into account in the solar aureole.

2.3. The MS-method

The preceding discussion suggests the possibility of further improvement of the DM-method by removal of the fluctuation induced by the delta-M method. As is well known for the successive-order scattering method,[16,21–24] the intensity field of an individual order of scattering becomes more isotropic and smoother when the scattering order increases.

This result is easily understood since the intensity secondarily scattered through a phase function $P(x) = P_L(x, g, M)$ approximately involves the following term:

$$P^2(x) = \int \mathrm{d}\Omega' \, P(\Omega \cdot \Omega')P(\Omega' \cdot \Omega_0) = \frac{1}{4\pi} \sum_{n=0}^{M} (2n+1) g_n^2 P_n(x). \tag{13}$$

Consequently, the moment of the field for higher-order Legendre polynomials is much smaller than that of the singly-scattered intensity field, because the moment is generally < 1 and a monotonically decreasing function of the order of the Legendre polynomial. In Fig. 1, we show the effective phase function P^2 for secondary scattering through the truncated phase function labelled DM. The figure shows that P^2 is a smooth and more isotropic function of the scattering angle than is the truncated phase function for single scattering.

Deirmendjian,[12] Box and Deepak,[13] and Arao and Tanaka[10] utilized this fact for intensity calculations in the solar aureole region. They showed that the Rayleigh phase function or a truncated phase function instead of the original phase function are sufficient for calculations of the multiply-scattered intensity field. Since the singly-scattered intensity dominates in the solar aureole region, an error introduced by this assumption is not so important in the solar aureole if we calculate the singly-scattered field exactly. In their methods, they used the Rayleigh or truncated phase functions for calculations of the multiple scattering field but with the original values of the optical depth and single-scattering albedo, in contrast to the truncation method. This approach is, however, inappropriate for calculations of intensities at large scattering angles and for optically-thicker atmospheres because of underestimation of the asymmetry of the phase function.

In order to compensate for this limitation, we used a slightly modified algorithm which applies the truncation theory. First, we calculate the intensity using a truncated transfer equation $\mathscr{T}(u^*, \omega^* P^*, \tau^*)$, from which we next subtract the singly-scattered intensity which satisfies the

equation $\mathscr{T}_1[\tilde{u}_1, (1-f)\omega P^*, \tau]$ and then add the exact solution u_1 given by Eq. (12):

$$u \approx u^* - \tilde{u}_1 + u_1 = u_m^* + u_1^* - \tilde{u}_1 + u_1, \tag{14}$$

where the u_m^* and u_1^* are, respectively, the multiply- and singly-scattered intensities in the solution of the truncated equation. This method has been adopted by Hansen and Pollack[25] to reduce the number of terms required in the Fourier expansion of the radiative intensity field with respect to azimuthal angle.

The percentage error in the resultant intensity calculated by the indicated method (hereafter referred to as the MS-method) is shown in the segment of Fig. 2 labelled MS. For scattering angles $>20°$, the error is well suppressed compared with the DM-method, while a large error remains in the solar aureole and transient regions.

2.4. *The TMS and IMS-methods*

From the results of the MS-method, we see that subtraction of the singly-scattered intensity cannot remove the fluctuation induced by the delta-M method, because the fluctuations result from the residue $u_1^* - \tilde{u}_1$ in Eq. (14). Alternatively, we synthesize the intensity as follows:

$$u' = u^* - u_1^* + \tilde{u}_1^* = u_m^* + \tilde{u}_1^*, \tag{15}$$

where $\tilde{u}_1^*$ is the solution of the equation $\mathscr{T}_1[\tilde{u}_1^*, \omega P/(1-f\omega), \tau^*]$. The intensity given by Eq. (15) involves the truncated phase function for secondary or higher orders of scattering. The segment of Fig. 2 labelled TMS shows the error in the resultant intensity u' obtained by this method (TMS-method). Compared with the MS-method, the error is substantially reduced for almost all scattering angles, other than those near the sun, where the intensity is overestimated in comparison with the MS-method.

To obtain a correction in the solar aureole region for the solution of the TMS-method, we use the equation for the deviation $\hat{u} = u - u'$ from Eqs. (1)–(3), (11) and (15) for the optically averaged homogeneous atmosphere:

$$\mu \, \mathrm{d}\hat{u}(\tau, \Omega)/\mathrm{d}\tau = -\hat{u}(\tau, \Omega) + \omega \int \mathrm{d}\Omega' \, P(\Omega \cdot \Omega')\hat{u}(\tau, \Omega') - J_1(\tau, \Omega) - J_2(\tau, \Omega) - J_3(\tau, \Omega), \tag{16}$$

where the additional negative source functions are given as

$$J_1(\tau, \Omega) = f\omega[u_m^*(\tau, \Omega) - \int \mathrm{d}\Omega' \, \hat{P}(\Omega \cdot \Omega')u_m^*(\tau, \Omega')], \tag{17}$$

$$J_2(\tau, \Omega) = \hat{\omega}\omega[P(\Omega \cdot \Omega_0)g(\tau^*, \mu, \mu_0) - \int \mathrm{d}\Omega' \hat{P}(\Omega \cdot \Omega')P(\Omega' \cdot \Omega_0)g(\tau^*, \mu', \mu_0)], \tag{18}$$

$$J_3(\tau, \Omega) = \omega P(\Omega \cdot \Omega_0)[\exp(-\tau^*/\mu_0) - \exp(-\tau/\mu_0)] - f\omega^*\omega \int \mathrm{d}\Omega' P^*(\Omega \cdot \Omega')\hat{P}(\Omega' \cdot \Omega_0)g(\tau^*, \mu', \mu_0), \tag{19}$$

$$\hat{\omega} = f\omega/(1-f\omega),$$

and the function g is the geometrical factor in Eq. (12) for the transmitted intensity through an averaged homogeneous atmosphere in the single scattering approximation

$$g(\tau, \mu, \mu_0) = \frac{\exp(-\tau/\mu)}{\mu} \int_0^\tau \mathrm{d}t \, \exp[(1/\mu - 1/\mu_0)t]. \tag{20}$$

In these equations, we assume an optically-averaged homogeneous atmosphere, because the correction is applied only to the solar aureole region, where an inhomogeneous structure of the atmosphere is unimportant because of small contribution from backward scattering.

The source function J_1 will be very small because the multiply-scattering field u_m^* is nearly constant around the direction of Ω_0 where the peaked phase function has significant non-zero values. The function J_2 will have significant values around the solar aureole for the same reason. Interpretation of the function J_3 is somewhat complex. Since the exponential function $\exp(-\tau^*/\mu_0)$

includes intensities that are multiply scattered through the forward peak, we should expand the exponential functions in Eq. (19) into successive orders of the single-scattering albedo as follows

$$\exp(-\tau^* m) - \exp(-\tau m) = -\exp(-\tau^* m) \sum_{n=1} (-f\omega\tau m)^n/n!, \tag{21}$$

where $m = 1/\mu_0$ is the optical air mass. With this procedure, Eq. (19) reduces to the following equation in the secondary scattering approximation:

$$J_3(\tau, \Omega) \approx \hat{\omega}\omega[P(\Omega \cdot \Omega_0) - (1-f) \int d\Omega' P^*(\Omega \cdot \Omega')\hat{P}(\Omega' \cdot \Omega_0)]g(\tau^*, \mu_0, \mu_0). \tag{22}$$

This result expresses a part of the light source caused by multiple scattering through the forward peak which is approximated by the delta function.

In conclusion, the following expression will be valid within the secondary scattering approximation, neglecting the angular integral in Eq. (16) and the source function J_1:

$$\hat{u}(\tau, \Omega) \approx -(1-f\omega)\hat{\omega}^2[2\hat{P}(\Omega \cdot \Omega_0) - \hat{P}^2(\Omega \cdot \Omega_0)]h(\tau, \mu, \mu_0^*, \mu_0^*), \tag{23}$$

where $\hat{P}^2$ is defined in Eq. (13) and

$$\mu_0^* = \mu_0/(1-f\omega).$$

The function h is given by

$$h(\tau, \mu, \mu', \mu_0) = \frac{1}{\mu} \int_0^\tau dt \exp[(t-\tau)/\mu)]g(t, \mu', \mu_0). \tag{24}$$

In manipulating the equations, we have brought the function g in Eqs. (18) and (19) outside of the angular integrals, and utilized the following equation that is valid in the delta-M method:

$$\int d\Omega' P^*(\Omega \cdot \Omega')\hat{P}(\Omega' \cdot \Omega_0) = P^*(\Omega \cdot \Omega_0). \tag{25}$$

The error in the intensity corrected by Eq. (23) is shown in the segment of Fig. 2 labelled IMS. The correction of Eq. (23) is sufficient in the solar aureole region, and the calculated intensity follows the exact values with an accuracy of better than 1.3% for all emergent directions.

3. NUMERICAL VALIDATION OF THE THEORY

3.1. Description of the simulation

In order to examine the accuracy of the various algorithms discussed in Sec. 2, we performed numerous solar radiative transfer computations. Models of seven polydispersions of Mie particles were assumed as summarized in Table 1. These polydispersions, expressed in terms of the volume spectrum $dV/d\ln r$, were used to compute the aerosol phase function for the particle radii r in the range 0.01–10 μm. JUNGE-4 and BIMODAL are polydispersions popularly used to model atmospheric aerosols.[26–29] JUNGE-3 is the optical equivalent of a soil-derived polydispersion containing large particles.[30,31] Values of the phase function and single-scattering albedo are calculated by Mie theory with the complex refractive index $\tilde{m}$ of $1.34 - 0i$ for CLOUD and $1.5 - 0i$ for other polydispersions as shown in Fig. 3.

In Fig. 4, we illustrate the coefficients g_n of the Legendre polynomial expansion of the phase function, as defined in Eq. (4). The behavior of the moments as a function of the order of the expansion is important in determining the required number N of discrete paths.[32] A comparison of Figs. 3 and 4 shows that phase functions containing a sharp forward peak (such as JUNGE-3 and CLOUD) require a larger number of Legendre coefficients to describe the phase function than those with only a modest forward peak (such as HAZE-L and HAZE-M). Consequently, an efficient truncation order varies with the type of polydispersion. A relatively low truncation order is suitable for the power-law type and CLOUD phase functions, because an increase of the truncation order is wasteful due to the persistent and slowly decreasing tails of the moments. On the other hand, a moderately large order is suitable for the truncation of haze type phase functions,

Table 1. Functional type and parameters of model volume spectra for Mie particles.

Type	$dV/d\ln r$
P	$C(r/r_0)^{4-p}$, p=0 for $r<r_0$
L	$\Sigma_{n=1,2} C_n \exp\{-[\ln(r/r_n)/\ln s_n]^2/2\}$
G	$Cr^{(\alpha+4)} \exp(-\beta r^{\gamma})$

Name	Type	Parameters
JUNGE-5	P	p=5, r_0=0.1μm
JUNGE-4	P	p=4, r_0=0.1μm
JUNGE-3	P	p=3, r_0=0.1μm
BIMODAL	L	r_1=0.132μm, s_1=1.55, C_1=4.8×10^{-12}
		r_2=2.16 μm, s_2=2.11, C_2=1.9×10^{-11}
HAZE-L	G	α=2, β=15.119, γ=0.5
HAZE-M	G	α=1, β= 8.944, γ=0.5
CLOUD	G	α=6, β= 1.500, γ=1.0

because the moment takes a large value at a low order, while it decreases rapidly as the truncation order increases.

Numerical computations of the radiative intensity were performed using a discrete ordinates method,[3] with a shifted double Gaussian quadrature.[1,19] All calculations were performed in double precision using FORTRAN 77 in order to avoid undesired computational errors not essential for the test. As the true value of the intensity, we tentatively used the intensity calculated by the MS-method with a sufficiently large number $N = N_{max}$ with truncation fractions $<1\%$ as shown in Table 2, where we also show the truncation fraction for various N.

Values of the solar zenith angle θ_0 and emergent angles (θ, ϕ) was assumed as follows:

$$\theta_0 = 0,\ 30,\ 60,\ 70,\ 78^\circ;\quad \phi = 0,\ 5,\ 10,\ 30\ (30)\ 150,\ 170,\ 175,\ 180^\circ;$$

$$|\theta - \theta_0| = 0\ (1)\ 10\ (2)\ 90^\circ. \tag{26}$$

The interpolation algorithm of Stamnes and Dale[8] was used to evaluate the intensity u_m^* for the TMS and IMS-methods, and u^* for other methods from values at discrete paths to arbitrary emergent directions.

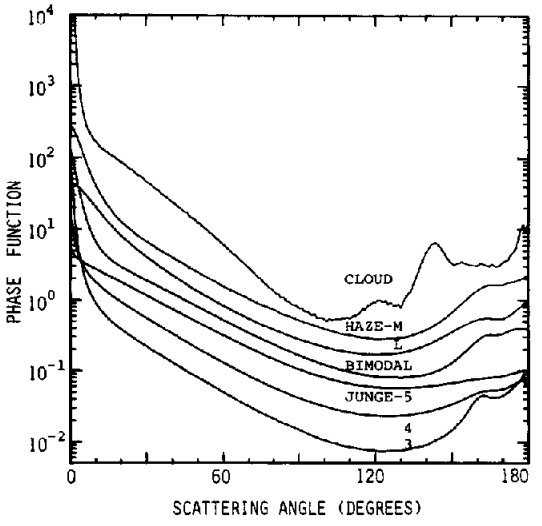

Fig. 3. Phase functions for the model polydispersions. Profiles are successively shifted upward by a factor of 2 for the first five phase functions and by a factor of 8 for CLOUD.

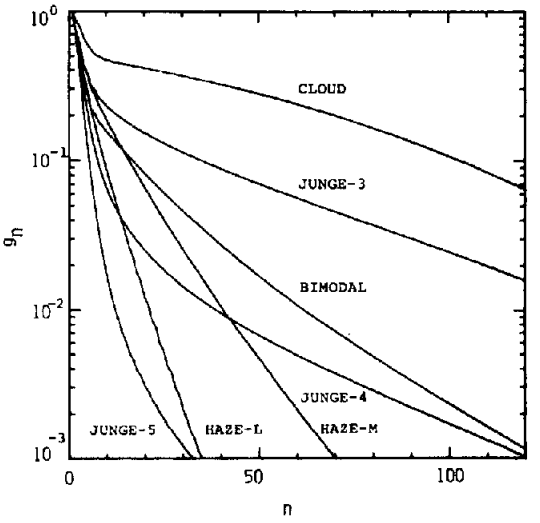

Fig. 4. Moments of the phase functions in Fig. 3 as a function of the order of Legendre expansion.

Table 2. Truncation fractions f_{max}, f_{20}, and f_{10} for $N = N_{max}$, 10 and 5.

Name	$2N_{max}$	f_{max}	f_{20}	f_{10}
JUNGE–5	60	0.00023	0.0028	0.0135
HAZE–L	60	0.00002	0.0109	0.0711
HAZE–M	80	0.00046	0.0605	0.1662
JUNGE–4	100	0.00166	0.0239	0.0570
BIMODAL	120	0.00111	0.0777	0.1444
JUNGE–3	180	0.00298	0.1479	0.2170
CLOUD	180	0.00844	0.4071	0.4601

The optical thickness of particulate matter $\tau_a = 0.2$, 0.8, and 3.2 was used for almost all tests. Since the optical thickness reaches about 0.6 in suburban areas of Japan in the summer season[33] and over the Chinese continent,[34] tests with $\tau_a = 0.8$ are required for testing remote sensing methods under such turbid conditions. The value of $\tau_a = 3.2$ and the CLOUD phase function are adopted for a preliminary test for an optically thick atmosphere. In all tests, we assumed the Rayleigh scattering optical thickness $\tau_R = 0.1434$ and the single-scattering albedo $\omega_R = 1$. This corresponds to a measurement at sea level pressure for a wavelength of 500 nm.

3.2. Tests in homogeneous atmospheres

Table 3 shows the maximum errors in the intensities for the emergent directions of Eq. (26), as calculated by the MS, IMS and GL-methods with $N = 10$. Apart from the CLOUD case, the maximum errors for the three methods presented in Table 3 are 20.5, 11.2 and 13.9% for transmission and 1.3, 1.7 and 5.4% for reflection, respectively, for $\tau_a \leqslant 3.2$. For $\tau_a \leqslant 0.8$, these errors are 20.5, 2.8 and 13.9% for transmission and 1.1, 1.3 and 4.8% for reflection, respectively. For the reflected intensity, there is no appreciable difference in accuracy between the MS and IMS-methods, both of which are more accurate than the GL-method. For the transmitted intensity, on the other hand, an assessment of the strengths and weaknesses of the various truncation approximations is more complex. Although we can say that the IMS-method is superior for calculations of the transmitted intensity for moderately thick atmospheres, an instability begins to occur as the optical thickness increases. This is clearly shown by large errors in the CLOUD model when $\tau_a = 3.2$, especially for large solar zenith angles. This error results from the large difference between the exponential functions in Eq. (19) for a large optical thickness. On the other hand, the other two methods are stable for all cases considered in Table 3. The GL-method is accurate for calculations of the transmitted intensity in cases other than HAZE-L and -M, but it does not work well for HAZE-L and -M, both of which have a broad phase function in the forward scattering direction, thereby negating the small angle approximation assumed in this method.

Investigation of the dependence of the relative error in the transmitted intensity on air mass and optical thickness shows that the errors tend to increase for increasing air mass for $\tau_a \leqslant 0.8$, while the errors decrease for large air masses for $\tau_a = 3.2$. This fact supports an expectation that the error becomes large at a moderately large effective optical path length of transmitted radiation. For other cases i.e., in the limits of small and large optical thicknesses, any algorithm under discussion is accurate due to dominance of the singly-scattered intensity or due to a redistribution of the radiant energy of the truncated peak by multiple scattering, respectively. As for the error in the reflected intensity, there is no significant dependence on either air mass or optical thickness. According to an investigation of the successive order theory,[23] contributions from relatively lower orders of scattering are dominant for the reflected flux even in thick atmospheres, while contributions of multiple scattering rapidly increase with increasing optical thickness for the transmitted flux.

The dependence of errors on air mass and the optical thickness is better demonstrated by angular distributions of the error shown in Fig. 5 for JUNGE-3, which is one of worst cases summarized in Table 3. In Fig. 5, the error is plotted as a function of the emergent zenith angle along the arch for each ϕ if $\theta > 0$ and $180 - \phi$ if $\theta < 0$. In the following similar figures, we show six error profiles without specifying the azimuthal angles since we are primarily concerned with the general tendency of the error. From Fig. 5, we see that principal sources of the maximum error in Table 3 are the

aureole and backscattering glory regions, although the angular region containing large errors depends significantly on the method of calculation. In the IMS-method, for example, a suppression of the fluctuation for large scattering angles is remarkable and regions of large errors are confined to scattering angles $\Theta \lesssim 10^\circ$ and $\Theta \gtrsim 170^\circ$ compared with other methods. Errors for large scattering angles are also small in the GL-method as compared with the MS-method, although systematic errors are not negligible around the horizon (as is expected from Fig. 2). Aside from small scattering angles, the computational error with $N = 10$ is $<0.5\%$ for almost all directions in the IMS-method, while errors comparable with the maximum appear over wide regions in the other two methods. For other optical thicknesses, the circumstances are similar to those in Fig. 5.

Although the angular dependences of errors are similar for other phase functions, as is shown in Fig. 6, the magnitudes vary significantly with the phase function. Errors for JUNGE-5 and HAZE-L with small truncation fraction are very small in the MS and IMS-methods. For other polydispersions, however, the intensity in the solar aureole fluctuates with an error as large as several percent in the MS-method. In the GL-method, systematic errors around the horizon are a common feature for all polydispersions, although the error in the aureole region is extensively suppressed, except for the HAZE-L and HAZE-M models, as seen in Table 3.

Figure 7 shows the error for various values of N with $\tau_a = 0.8$ and the JUNGE-3 model. The convergence with increasing N is very slow for the MS-method, as is expected from the behavior of the Legendre moments illustrated in Fig. 4. This occurrence is similar in the IMS-method, but

Table 3. Maximum relative errors in transmitted (A) and reflected (B) intensities for $N = 10$; the unit in 1/1000.

(A)		τ=0.2			τ=0.8			τ=3.2		
Name	θ_0	MS	IMS	GL	MS	IMS	GL	MS	IMS	GL
JUNGE	0	0	0	3	0	0	3	0	0	3
−5	30	1	1	3	1	1	3	1	1	3
	60	1	1	3	0	1	3	0	0	4
	70	1	1	3	1	1	4	1	1	4
	78	1	1	4	1	1	5	1	1	3
HAZE-L	0	1	0	17	2	1	17	4	2	16
	30	1	1	18	1	1	19	2	1	17
	60	1	1	17	1	1	19	2	1	22
	70	1	1	18	2	1	24	1	1	19
	78	1	1	20	2	1	44	1	1	19
HAZE-M	0	3	2	31	12	5	35	35	8	32
	30	4	2	33	12	5	37	31	5	33
	60	6	2	32	19	3	36	27	3	43
	70	8	2	34	25	3	47	12	3	38
	78	13	2	37	34	7	139	3	3	37
JUNGE	0	1	1	8	5	1	9	12	1	9
−4	30	1	1	9	5	1	10	12	1	9
	60	2	1	9	8	1	9	10	1	11
	70	3	1	9	11	1	11	3	1	10
	78	5	1	10	15	1	21	1	1	10
BIMODAL	0	5	1	17	21	3	19	62	5	19
	30	6	2	18	23	3	20	62	5	19
	60	10	2	18	38	2	20	62	11	22
	70	16	2	18	53	2	23	30	10	21
	78	27	2	19	73	8	80	2	2	20
JUNGE	0	15	2	20	55	3	23	173	17	22
−3	30	17	2	22	64	2	26	183	26	23
	60	30	2	23	103	4	27	195	78	29
	70	44	2	24	143	10	33	128	112	26
	78	73	3	24	205	28	119	7	7	25
CLOUD	0	72	4	13	245	19	17	555	143	30
	30	91	7	18	293	34	30	606	217	49
	60	148	4	22	416	38	34	648	838	147
	70	208	7	19	507	77	27	582	1977	247
	78	317	19	35	618	238	46	162	1415	149

Table 3—*continued*

(B)		τ=0.2			τ=0.8			τ=3.2		
Name	θ_0	MS	IMS	GL	MS	IMS	GL	MS	IMS	GL
JUNGE	0	0	0	3	0	0	4	0	0	3
−5	30	1	1	4	0	0	4	1	1	4
	60	1	1	4	1	1	5	1	1	5
	70	1	1	3	1	1	4	1	1	5
	78	1	1	3	1	1	4	1	1	4
HAZE-L	0	0	0	18	1	1	21	1	1	19
	30	1	1	19	1	1	23	2	2	23
	60	1	1	19	1	1	25	1	1	28
	70	1	1	18	1	1	26	1	1	29
	78	1	1	15	1	1	22	1	1	25
HAZE-M	0	1	1	33	2	3	40	2	3	39
	30	3	3	34	5	4	44	5	5	45
	60	3	2	34	4	3	48	5	4	53
	70	3	3	32	5	4	47	5	4	54
	78	5	3	29	8	4	45	9	5	52
JUNGE	0	0	0	9	1	0	10	1	1	10
−4	30	1	1	9	1	1	12	1	1	12
	60	1	1	9	1	1	13	1	1	14
	70	1	1	9	1	1	13	1	1	15
	78	1	1	8	1	1	11	1	1	13
BIMODAL	0	1	1	18	2	1	22	2	2	22
	30	2	2	18	4	3	24	4	2	25
	60	2	2	19	3	3	26	4	3	30
	70	2	2	17	4	3	25	4	3	29
	78	5	2	16	8	3	25	9	4	28
JUNGE	0	2	3	20	8	13	24	9	13	24
−3	30	3	3	22	8	12	29	8	11	30
	60	3	4	22	8	13	31	9	13	35
	70	4	5	21	9	13	31	10	15	36
	78	7	5	20	11	13	33	13	17	39
CLOUD	0	10	8	10	51	39	44	71	50	58
	30	11	6	16	51	29	44	64	38	53
	60	14	8	18	50	30	42	54	34	44
	70	18	10	16	51	31	43	60	37	48
	78	21	12	21	54	32	46	71	43	58

the error is much smaller for all emergent angles compared with the MS-method. It is remarkable that the error for $N = 5$ is $<0.5\%$ for almost all emergent angles in the IMS-method. An increase of discrete paths contributes primarily to reduction of the error in large scattering angles, especially around the horizon.

3.3. Tests in inhomogeneous atmospheres

The indicated simulations were all performed for homogeneous atmospheres. To see whether the IMS-method works well in inhomogeneous atmospheres, we show an example of such simulation in Fig. 8. The following two sublayers were assumed:

$$\text{layer 1, } \tau_{a1} = 0.1\,\tau_a, \quad \tau_{R1} = 0.7\,\tau_R, \quad \tilde{m} = 1.5 - 0.03i;$$

$$\text{layer 2, } \tau_{a2} = 0.9\,\tau_a, \quad \tau_{R2} = 0.3\,\tau_R, \quad \tilde{m} = 1.5 - 0.03i.$$

This model corresponds to an atmosphere with a haze layer of 3 km thickness including absorbing aerosols. In Fig. 8, we assume $\tau_a = 0.8$, $\tau_R = 0.1413$ and the JUNGE-4 polydispersion. Although such inhomogeneity causes large changes in the radiation regime compared with the homogeneous equivalence, as shown by broken lines, the error in the IMS-method is as small as in the homogeneous cases. From the figure we also see that it is valid to assume the homogeneous approximation for the correction of Eq. (16) in the solar aureole region.

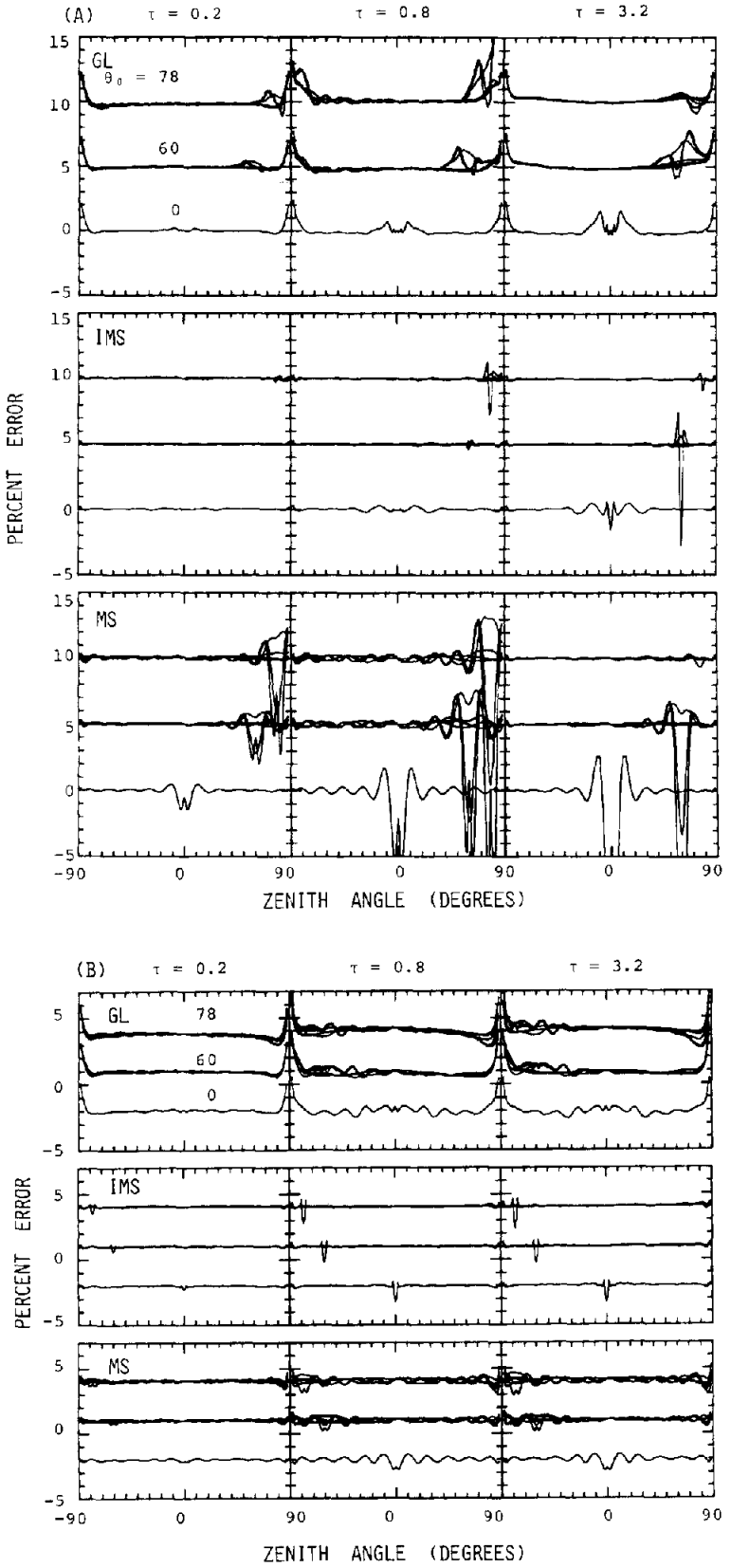

Fig. 5. Angular dependence of the percentage error in the transmitted (A) and reflected (B) intensities calculated by GL, MS, and IMS-methods with $N = 10$, $\theta_0 = 0$, 60, 78° and $\tau_a = 0.2$, 0.8, and 3.2 for JUNGE-3. Profiles for various solar incidences are successively shifted by 5 and 3% in (A) and (B), respectively.

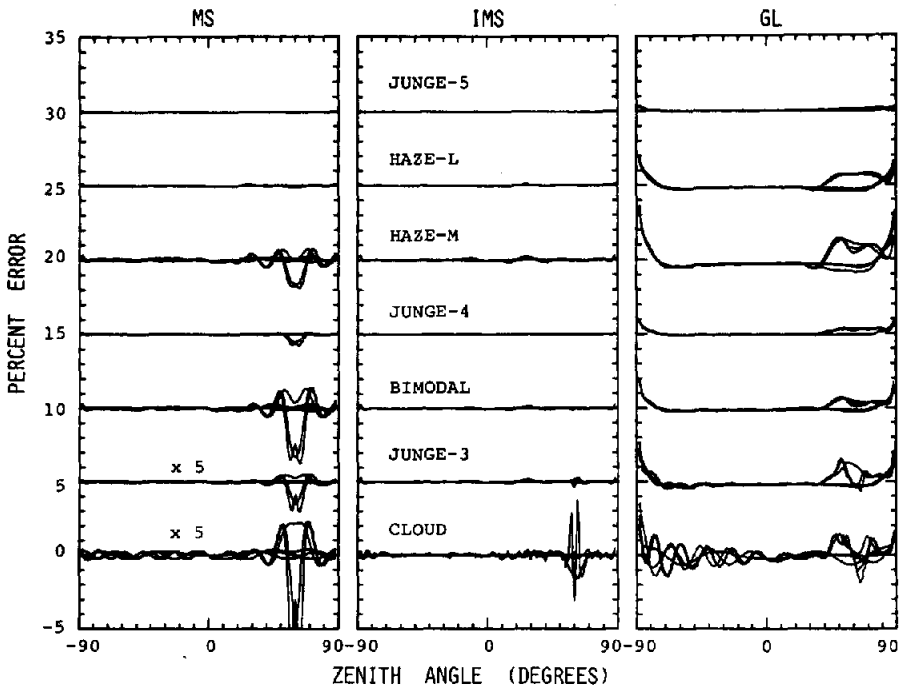

Fig. 6. Percentage errors in the transmitted intensities for various phase functions (successively shifted by 5%); $N = 10$, $\tau_a = 0.8$ and $\theta_0 = 60°$. Scales for JUNGE-3 and CLOUD are 5 times the indicated values.

Although not presented in the figure, a similar simulation with the JUNGE-3 model also demonstrates the validity of the IMS-method. In this case, larger errors of ~0.5% are found in the aureole region at high solar elevation, while the reflected intensity is more accurate than that for a homogeneous case with $\tilde{m} = 1.5 - 0i$, because the phase function for absorbing aerosols does not have a distinct backscattering glory.

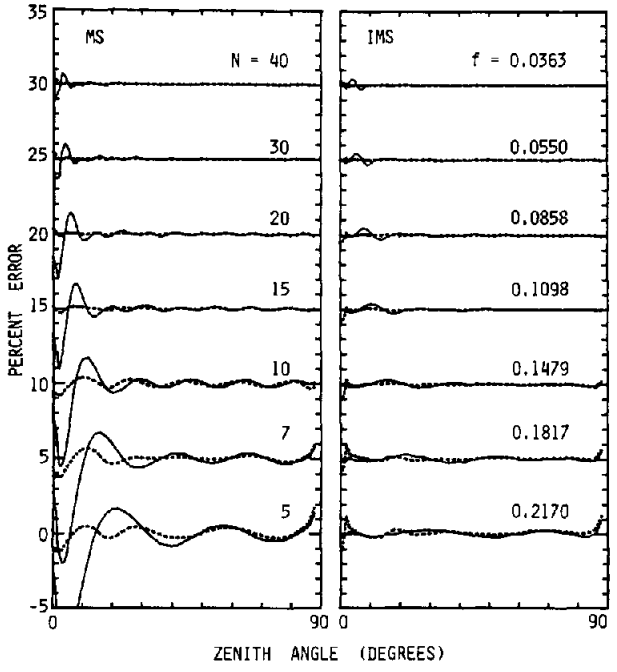

Fig. 7. Percentage error for $N = 5$, 7, 10, 15, 20, 30, and 40 (successively shifted upward by 5%). Solid and broken lines are for transmission and reflection, respectively; $\tau_a = 0.8$ and $\theta_0 = 0°$, and JUNGE-3.

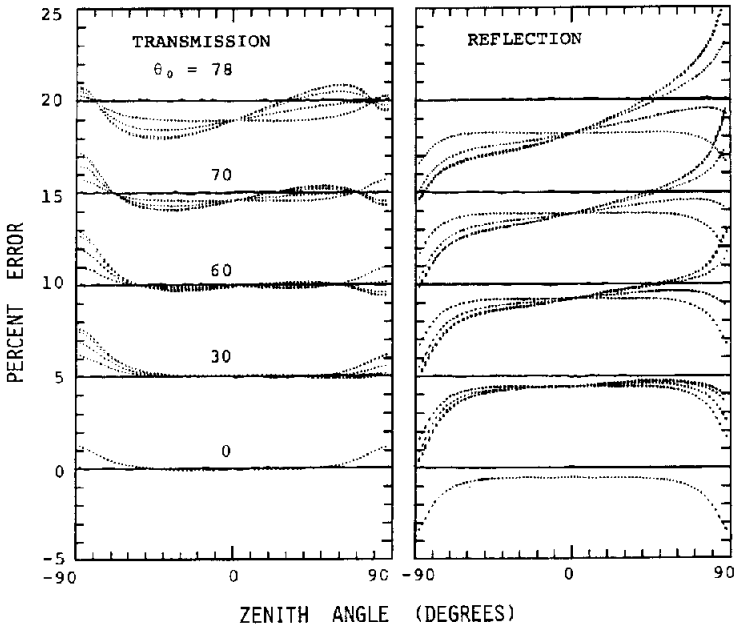

Fig. 8. Percent deviation of the intensity in an inhomogeneous atmosphere from the homogeneous case (broken lines with a scale of 1/10) and percentage error in the method with $N = 10$ (solid lines). Profiles for various solar zenith angles are shifted upward by 5%.

4. DISCUSSION

In the preceding sections, we demonstrated that the IMS-method can give accurate radiative intensity fields in aerosol-laden atmospheres for optical thicknesses $\lesssim 1$ with a relatively small number of discrete paths. Since this agreement is possible because the multiply-scattered intensity is a smooth and not strongly anisotropic function of emergent angles, we are able to find a close relation with past investigations on the efficiency of computational algorithms for radiative transfer calculations.

Many investigators have paid attention to the number of Fourier terms necessary for accurate calculation of the intensity field.[10,25,32,35,36] These authors have pointed out that the number of Fourier terms required for accurate intensity calculations is much less than the number of Legendre polynomials necessary for accurate computation of particle phase function. This result is caused primarily by two effects: one is that an analytically smooth function of spherical coordinates is symmetric around the axis of rotation and this property is reflected in the fact that the associated Legendre polynomial $P_n^m(x)$ decreases rapidly as x approaches 1; the other reason is that an intensity field, other than that for single scattering, is a weak function of emergent angles.

As for the second reason, it is peculiar that there have been few investigations of the necessary number of discrete paths of the zenith angle, because this number is closely related to the necessary number of Fourier terms needed for the addition theorem of spherical harmonics. Arao and Tanaka[10] used 5–20 Fourier terms in their aureole calculations, while they used 28 discrete paths of the zenith angle in the hemisphere. We show from the following discussion that a suitable number of discrete paths is also reduced considerably in the IMS-method.

Arao and Tanaka related the necessary number of Fourier terms, with an error of 0.5% in the aureole intensity, to the magnitude $P(0)$ of the forward peak of the phase function, as is shown by the broken line in Fig. 9. In the same figure, we also show the truncation order M^* in Eq. (5) with the truncation fraction $f = 0.1$ for various phase functions, with a regression line of

$$M^* = 3.77P(0)^{0.553}. \tag{27}$$

Since the magnitude of the forward peak correlates well with the truncation fraction, we see from Fig. 9 that the criterion of Arao and Tanaka is equivalent to the assumption of a truncation fraction

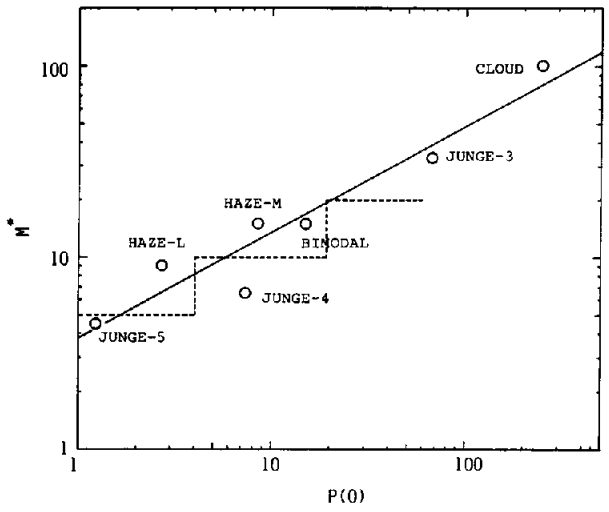

Fig. 9. Relation between the magnitude of the forward peak of the normalized phase function and the truncation order for $f = 0.1$. The solid line is the regression line of Eq. (27) and the broken line is the number of Fourier terms necessary for the intensity calculation with an error <0.5% in the method of Arao and Tanaka.

<0.1. King[32] showed that the necessary number of discrete paths of the zenith angle for accurate radiative transfer calculations is approximately equal to $0.35M$; therefore, phase functions with a large forward peak (large M^*) require a large number of discrete paths. We were thus motivated to examine the computational error in the emerging intensity arising from various quantities of the scattering system, viz., the truncation fraction f, scattering optical thickness $\omega\tau$, air mass m, and attenuation rate of the incident beam $\exp(-\tau m)$ as follows:

$$E = Cf^{\alpha}(\omega\tau)^{\beta}m^{\gamma}\exp(-\delta\tau m), \tag{28}$$

where E is the maximum error in emergent intensities for each solar incident direction. Since the error in the solar aureole E_a and in the backscattering glory E_b are of different character, we analyze the maximum errors in four regions of the sky:

$$E_t = E_a + E_d \quad \text{and} \quad E_r = E_b + E_u, \tag{29}$$

where E_t and E_r are maximum errors in the transmitted and reflected intensities, and E_d and E_u are maximum errors in those intensities outside of the solar aureole ($\Theta \leqslant \Theta_0$) and the backscattering glory ($\Theta \geqslant 180 - \Theta_0$); the critical scattering angle Θ_0 is 10° for the CLOUD model and 5° for other polydispersions. In Table 4 and Fig. 10, we show the result of our regression analyses using the IMS-method and Eq. (28) for E_d, E_u, E_a, and E_b. For the analyses, we used data of the maximum error in Table 3, similar data with $N = 5$, data in Fig. 7, and data in Fig. 8 for JUNGE-4 and -3. Since we found that the statistics of E_d and E_u were similar, coefficients interpreting both errors are shown in Table 4. These errors are most strongly dependent on the truncation fraction, with other parameters having reduced importance. On the other hand, we found that E_a varies approximately as $(f\omega\tau m)^3$, as is expected from Eq. (21) since the correction in Eq. (23) is valid within the secondary scattering in the solar aureole region. Similarly, an exponent around 1 for f and a small exponent for δ in the parameterization of E_b are reasonable since the IMS-method can induce an error even in the singly-scattered intensity if the truncated phase function deviates significantly from the original function.

From Eq. (28) and Table 4, we find that introduction of a truncation fraction of 0.1 in an atmosphere of optical thickness 0.4 and air mass of 1, as in the model of Arao and Tanaka,[10] is expected to yield an error of 0.4% in the IMS-method. This estimate is about same as the value determined from the criterion of Arao and Tanaka. Figure 4 shows that the required number of discrete paths for $f = 0.1$ is $N = 18$ for the JUNGE-3 while $N \leqslant 10$ for other aerosol models. In the IMS-method, therefore, the number of discrete paths can be reduced to a value much less than

Table 4. Regression coefficients of maximum percentage errors in Eq. (28).

Error	C	α	β	γ	δ
E_d, E_u	1.8	0.62	0.09	0.28	0.016
E_a	45.6	3.36	2.82	2.90	0.245
E_b	5.0	1.34	0.34	0.54	0.035

the necessary number of Legendre polynomials needed to expand the phase function, and this finding is consistent with past investigations about the necessary number of Fourier terms. This finding is important because the computational time is approximately proportional to $N^2 \sim N^{2.5}$ in the discrete ordinates method and N^3 in the matrix operator method. On the other hand,

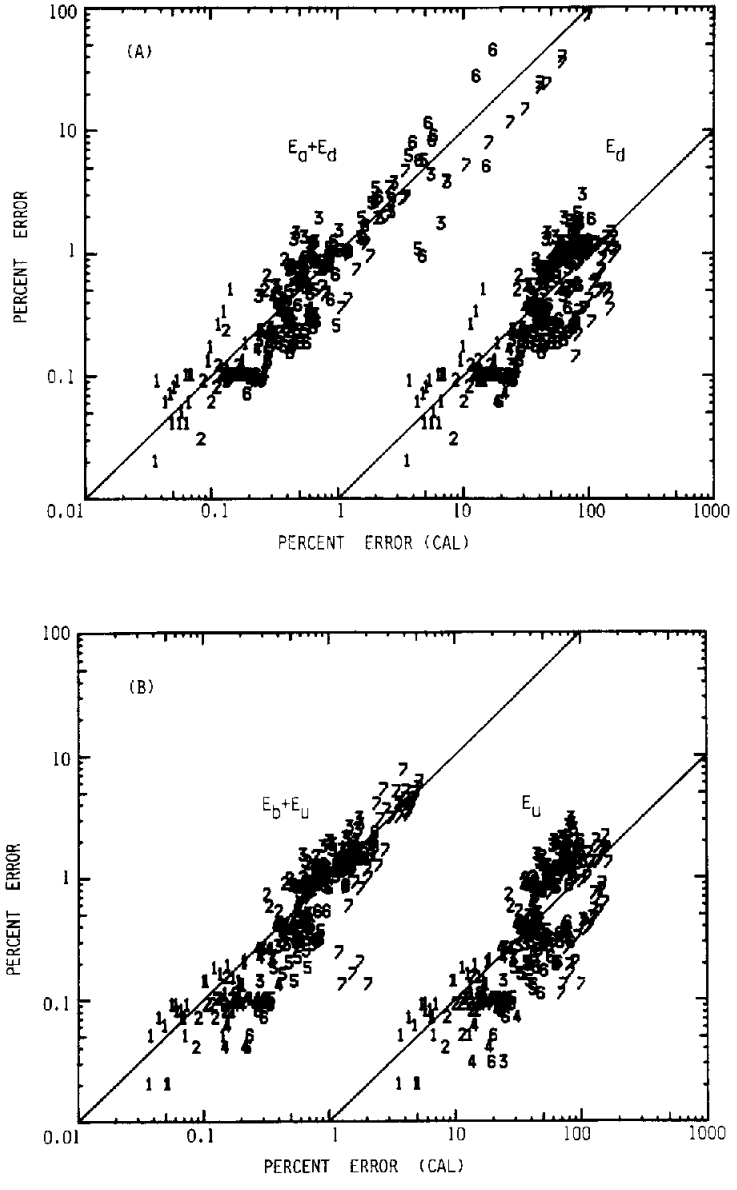

Fig. 10. Simulated (ordinate) and calculated percentage errors from Eq. (28) (abscissa) for transmitted (A) and reflected (B) intensities in the IMS-method. Symbols denote the phase function (1—JUNGE-5; 2—HAZE-L; 3—HAZE-M: 4—JUNGE-4: 5—BIMODAL: 6—JUNGE-3: 7—CLOUD). Plots of E_d and E_u are shifted right by a factor of 100.

convergence of the Fourier expansion of the intensity field in azimuthal angle can be monitored in the course of the computation, so that no *a priori* knowledge of the necessary number of Fourier terms is needed.

For an application of the IMS-method to planetary atmospheres, we must also consider the polarization effect caused by the large polarizability of atmospheric molecules. The error of neglecting polarization effects in radiative transfer increases with a decrease of the wavelength, reaching about 7% at 320 nm even in the total intensity.[18,37] Although it is possible to extend the IMS-method to the solution of radiative transfer problems including the Stokes vector, we recommend a simple correction scheme recently developed by Ogawa et al[37] if we need the total intensity alone. Since the error in the correction is at most 0.5%, we can have an intensity field in a realistic plane-parallel atmosphere with an error $<1\%$ for all emergent directions in the moderately thick atmosphere using the IMS-method with a reasonable number of discrete paths.

In order to perform an angular interpolation of emergent zenith angles, we also used a cubic spline interpolation. Although this interpolation works well for $N \gtrsim 15$, notable errors are produced as N decreases. In particular, errors as large as several percent appear around the transient regions of the solar aureole and horizon for the normal incidence. On the other hand, the interpolation of Stamnes and Dale[8] is very stable for arbitrary emergent angles. For the TMS and IMS-methods, the interpolation can be directly applied to the multiply-scattered intensity as shown in the Appendix. We can apply these schemes to the new calibration algorithm of the sunphotometer,[38] which requires an accurate circumsolar intensity at a scattering angle of 20° and air masses <5. A very small number of discrete paths in the hemisphere around $N = 5$ is sufficient for such a calculation for normal conditions when JUNGE-4 type aerosols prevail.

5. SUMMARY

We have examined the computational accuracy of various intensity calculation schemes. The following are our salient results: (1) The intensity calculated by the DM-method leads to large errors because of fluctuations involved in the phase function truncated by the delta-M method. (2) Synthesis of the singly- plus multiply-scattered intensities, as in the MS-method, also leads to errors caused by phase function fluctuations. (3) Similar syntheses using the scaled variables of Eq. (3), such as the TMS and IMS-methods, suppress the errors substantially. (4) The second order correction in Eq. (23) is valid for moderately thick atmospheres and the maximum error is well predicted by Eq. (28), where the regression coefficients are given in Table 4. Finally, the IMS-method is the best method we have found for calculating the transmitted and reflected intensities in moderately thick atmospheres with an optical thickness $\lesssim 1$.

Acknowledgement—The authors express their gratitude to K. Stamnes, S.-C. Tsay, and M. D. King for valuable discussions.

REFERENCES

1. K. Stamnes and R. A. Swanson, *J. Atmos. Sci.* **38,** 387 (1981).
2. K. Stamnes, S.-C. Tsay, and T. Nakajima, *JQSRT* **39,** 415 (1988).
3. T. Nakajima and M. Tanaka, *JQSRT* **35,** 13 (1986).
4. A. H. Karp, J. Greenstadt, and J. A. Fillmore, *JQSRT* **24,** 391 (1980).
5. A. H. Karp and S. Petrack, *JQSRT* **30,** 351 (1983).
6. Y. Takeuchi, *JQSRT* **39,** 237 (1988).
7. W. J. Wiscombe, *J. Atmos. Sci.* **34,** 1408 (1977).
8. K. Stamnes and H. Dale, *J. Atmos. Sci.* **38,** 2696 (1981).
9. T. Nakajima, M. Tanaka, and T. Yamauchi, *Appl. Opt.* **22,** 2951 (1983).
10. K. Arao and M. Tanaka, *J. Met. Soc. Jap.* **64,** 743 (1986).
11. J. F. Potter, *J. Atmos. Sci.* **27,** 943 (1970).
12. D. Deirmendjian, *Ann. Geophys.* **15,** 218 (1959).
13. M. A. Box and A. Deepak, *J. Atmos. Sci.* **38,** 1037 (1981).
14. J. T. Twitty, R. J. Parent, J. A. Weinman, and E. W. Eloranta, *Appl. Opt.* **15,** 980 (1976).
15. T. Nakajima, M. Tanaka, T. Hayasaka, Y. Miyake, Y. Nakanishi, and K. Sasamoto, *Appl. Opt.* **25,** 4374 (1986).
16. H. C. van de Hulst, *Multiple Light Scattering, Tables, Formulas, and Applications*, Vols. 1 and 2, Academic Press, New York, NY (1980).

17. M. D. King, *J. Atmos. Sci.* **38,** 2031 (1981).
18. S. Chandrasekhar, *Radiative Transfer*, Dover, New York, NY (1960).
19. M. Tanaka and T. Nakajima, *JQSRT* **18,** 93 (1977).
20. J. A. Weinman, J. T. Twitty, S. R. Browning, and B. M. Herman, *J. Atmos. Sci.* **32,** 577 (1975).
21. J. S. Goldstein, *Astrophys. J.* **132,** 473 (1960).
22. K. I. Gross, *J. Math. Phys.* **41,** 53 (1962).
23. M. Tanaka, *Sci. Rep. Tôhoku Univ., Ser. 5* **17,** 125 (1966).
24. H. C. van de Hulst, *JQSRT* **11,** 785 (1971).
25. J. E. Hansen and J. B. Pollack, *J. Atmos. Sci.* **27,** 265 (1970).
26. O. B. Toon and J. B. Pollack, *J. Appl. Met.* **15,** 225 (1976).
27. E. M. Patterson and D. A. Gillette, *J. Geophys. Res.* **82,** 2074 (1977).
28. M. Tanaka, T. Takamura, and T. Nakajima, *J. Clim. Appl. Met.* **22,** 1253 (1983).
29. T. Nakajima, T. Takamura, M. Yamano, M. Shiobara, T. Yamauchi, R. Goto, and K. Murai, *J. Met. Soc. Jap.* **64,** 765 (1986).
30. C. Tomasi, V. Vitale, and E. Caroli, *J. Aerosol Sci.* **14,** 529 (1983).
31. K. Arao and Y. Ishizaka, *J. Met. Soc. Jap.* **64,** 79 (1986).
32. M. D. King, *JQSRT* **30,** 143 (1983).
33. M. Tanaka, T. Nakajima, M. Shiobara, and T. Hayasaka, *Proc. of Beijing International Radiation Symposium*, Beijing (1988).
34. J. Qiu and Z. Xiuji, *Adv. Atmos. Sci.* **3,** 341 (1986).
35. J. V. Dave and J. Gazdag, *Appl. Opt.* **9,** 1457 (1970).
36. J. E. Hansen and L. D. Travis, *Space Sci. Rev.* **16,** 527 (1974).
37. H. Ogawa, M. Tanaka, and T. Nakajima, Submitted to *Appl. Opt.* (1988).
38. M. Tanaka, T. Nakajima, and M. Shiobara, *Appl. Opt.* **25,** 1170 (1986).
39. G. N. Plass, G. W. Kattawar, and F. E. Catchings, *Appl. Opt.* **12,** 314 (1973).

APPENDIX

We briefly summarize the matrix formulations for intensity calculations based on the algorithm of Nakajima and Tanaka[3] (hereafter referred as NT) and Stamnes and Dale.[8]

We approximate an inhomogeneous atmosphere by L-sublayers of an optically-homogeneous atmosphere. The reflection and transmission matrices of each layer are given by

$$\begin{bmatrix} R \\ T \end{bmatrix} = A^{+}C_{11} \pm B^{+}C_{22} \tag{A1}$$

and the source matrices by

$$\epsilon^{\pm} = A^{+}\alpha \pm B^{+}\beta + V^{\pm}E_0(\tau^{\pm}). \tag{A2}$$

In these expressions, + and − denote the downward and upward directions, respectively; $\tau^{+} = \tau_1$ is the thickness of the sublayer, and $\tau^{-} = 0$. The matrices which appear in Eqs. (A1) and (A2) have been given in Eqs. (36), (37), (40), (43) and (44) of NT with some modification of the following matrix inversion because of computational stability for large N:

$$C_{11} = \tfrac{1}{2}(\sqrt{WM}\,A^{-})^{-1}\sqrt{WM} \quad \text{and} \quad C_{22} = \tfrac{1}{2}(\sqrt{WM}\,B^{-})^{-1}\sqrt{WM}. \tag{A3}$$

Using the adding theory of the matrix operator method,[39] we have the internal intensities $u^{+}(0)$ and $u^{-}(\tau_1)$ at each interface of the sublayers. The integration constants α and β, which appear in Eq. (A2), are given by

$$\alpha = C_{11}[u^{-}(\tau_1) - V^{-}E_0(\tau_1) + u^{+}(0) - V^{-}],$$

and

$$\beta = C_{22}[u^{-}(\tau_1) - V^{-}E_0(\tau_1) - u^{+}(0) + V^{+}]. \tag{A4}$$

The intensity at an arbitrary optical depth is then given by

$$u^{\pm}(\tau) = A^{\pm}(\tau)\alpha + B^{\pm}(\tau)\beta + V^{\pm}E_0(\tau). \tag{A5}$$

For interpolation of the calculated intensities to an arbitrary emergent direction (μ', ϕ'), we use the general solution of Eq. (1) following Stamnes and Dale:

$$u'^{\pm}(\tau) = E'(\tau_b - \tau_a)u'^{\pm}(0) + M'^{-1}\int_{\tau_a}^{\tau_b} dt\, E'(|t - \tau|)J'^{\pm}(t), \tag{A6}$$

where $\tau_a = 0$ and $\tau_b = \tau$ for u'^+ and $\tau_a = \tau$ and $\tau_b = \tau_1$ for u'^-. In this expression, matrices with $'$ show the quantities for the direction (μ', ϕ'). For example, M' is the diagonal matrix in Eq. (NT6) but with μ', i.e. $M'_{ij} = \{\mu'_i \delta_{ij}\}$. After some manipulation of the formulations of NT, we have the following expression for the second term in Eq. (A6):

$$\Delta u'^{\pm}(\tau) = M'^{-1}\{[H * \overline{C(\tau)} \mp \tilde{H} * \overline{LS(\tau)}]\alpha + [H * \overline{L^{-1}S(\tau)} \mp \tilde{H} * \overline{C(\tau)}]\beta + [P'^{\pm} WV^{+} + P'^{\mp} WV^{-} + sw \cdot S'^{\pm} E_0(\tau)]\overline{E_0(\tau)}\}, \quad \text{(A7)}$$

where

$$H = (P'^{+} + P'^{-})\sqrt{W/M}\, Q \quad \text{and} \quad \tilde{H} = (P'^{+} - P'^{-})\sqrt{W/M}\, \tilde{Q}. \quad \text{(A8)}$$

Matrices $P'^{\pm}$ and $s'^{\pm}$ are given in Eqs. (8) and (9) of NT but for the emergent direction μ'_i instead of μ_i, and matrices Q, $\tilde{Q}$, L, $C(\tau)$ and $S(\tau)$ are given in Eqs. (23), (35), (28), (30) and (31) of NT. Quantities labelled by a horizontal bar are given by the following definition:

$$(\overline{C(\tau)})_{ijk} = \int_{\tau_a}^{\tau_b} dt \exp(-|t - \tau|/\mu'_i) C_{jk}(t) \quad \text{(A9)}$$

as for the function $C(\tau)$ in Eq. (NT30) for example. The matrix operation denoted by * is defined as follows:

$$H \cdot \overline{C(\tau)} = \left\{\sum_j H_{ij}[\overline{C(\tau)}]_{ijk}\right\}. \quad \text{(A10)}$$

Switch sw in Eq. (A7) is 0 for the interpolation of the multiply-scattered intensity in the TMS and IMS-methods, and equal to 1 in other cases.